

Research Article

Development and Evaluation of Amlodipine-Polymer Nanocomposites Using Response Surface Methodology

Zain Alabden Ghanim Ahmed,^{1,2} Samer Hasan Hussein-Al-Ali ^{1,3},
Ibrahim Abdel Aziz Ibrahim,⁴ Mike Kh. Haddad,⁵ Dalia Khalil Ali,^{1,6}
Anwar Mahmoud Hussein,¹ and Ahmad Adnan Abu Sharar⁷

¹Department of Basic Pharmaceutical Sciences, Faculty of Pharmacy, Isra University, Amman 11622, Jordan

²Ibn Al-Atheer Teaching Hospital, Nineveh Health Directorate, Nineveh, Iraq

³Department of Chemistry, Faculty of Science, Isra University, Amman 11622, Jordan

⁴Department of Pharmacology and Toxicology, Faculty of Medicine, Umm Al-Qura University, Makkah, Saudi Arabia

⁵Department of Renewable Energy Engineering, Faculty of Engineering, Isra University, Amman 11622, Jordan

⁶Department of Physiotherapy, Faculty of Allied Medical Sciences, Isra University, Amman 11622, Jordan

⁷Research and Development (R&D) Department, Hikma Pharmaceutical Inc., Amman 11118, Jordan

Correspondence should be addressed to Samer Hasan Hussein-Al-Ali; sameralali72@yahoo.com

Received 8 June 2022; Revised 19 August 2022; Accepted 22 August 2022; Published 20 September 2022

Academic Editor: Ahmed Tayel

Copyright © 2022 Zain Alabden Ghanim Ahmed et al. This is an open access article distributed under the Creative Commons Attribution License, which permits unrestricted use, distribution, and reproduction in any medium, provided the original work is properly cited.

Introduction. Polymer nanoparticles are a key tool to deliver drugs to specific sites and to increase drug bioavailability. *Aim.* This research aims to use poly amide-disulfide nanoparticles as drug delivery systems. *Method.* Amlodipine (Amlop) was used as a model, forming Amlop-polymer nanocomposites. In this work, we investigated the effect of independent variables (polymer, Fe^{3+} , Al^{3+} , and pH) on the dependent variables (loading efficiency (%LE), zeta potential, and particle size). Nanocomposites were prepared by an inotropic method. Nanocomposites were characterized by powder X-ray diffraction (PXRD), field emission scanning electron microscopy (FE-SEM), Fourier transform infrared spectroscopy (FTIR), and a release study. *Results.* From the XRD data, the Amlop-polymer nanocomposite shows semi crystallinity. In addition, the disappearance of drug peaks indicates that the drug was incorporated between the polymer molecules and was amorphous in behavior. The FTIR for the nanocomposite shows the functional group of the drug, which indicates the incorporation of Amlop into the nanocomposite. From FE-SEM, the results showed that our nanocomposites have an average particle size of approximately 130 nm. The release of amlodipine from the Amlop-polymer nanocomposite was found to be controlled, with approximately 85% within approximately 24 hours. *Conclusion.* The amide-disulfide polymer nanoparticles are promising carriers for different types of drugs.

1. Introduction

Recently, research has focused on creating biodegradable nanoparticles for drug delivery [1]. For this purpose, various polymers have been used, as they can efficiently transfer the drug to a target location and thereby improve the therapeutic advantage while reducing adverse effects [2, 3]. Therefore, the major objective in the use of polymers in drug delivery is the controlled release of therapeutics to the specific action site at the clinically optimal rate and dosage regimen [4].

Biodegradable polymers draw interest as they can be transformed into nontoxic monomers, and a continuous rate of drug release can be obtained from degradable polymer-based sustained delivery [5].

The most common polymers used in drug delivery systems are chitosan [6, 7], cyclodextrin [8], alginate [7, 9], and polyamides and disulfide linkages [10]. However, more new polymer systems now exist that incorporate additional features for targeted delivery or combination therapies.

Nanoparticles are broad types of materials that involve particulate substances that possess one dimension lower than 100 nm [11]. Nanoparticles can be classified into various classes depending on their shapes, properties, and sizes [11]. Nanoparticles have been utilized for a variety of applications, including the delivery of diagnostic and therapeutic agents [12].

Amlodipine is a third-generation dihydropyridine calcium channel blocker that acts by preventing the absorption of calcium into smooth muscle cells and myocardial cells, resulting in reduced vascular peripheral resistance [13]. Amlodipine is already commonly used clinically for the prevention of a number of cardiovascular conditions, including angina pectoris and critical hypertension [14].

There are many recent studies in which nanotechnology has been used to deliver amlodipine; for example, Alawdi investigated the loading of amlodipine on nanodiamond particles [15]. The emulsion solvent evaporation method was employed successfully to produce the amlodipine-PLGA nanoparticles [16]. The transdermal system containing amlodipine-pluronic was investigated and enhanced transdermal permeation of the poorly water-soluble drug via transdermal films [17]. Amlodipine-gold nanoparticles were also investigated as a new "Turn off-on" sensor for the sensitive determination of methimazole [18].

The present work contains a polymer prepared in the laboratory with polyamide and disulfide structures. It is used for the first time in drug delivery. The polyamide and disulfide polymer are degradable by glutathione and sensitive to pH. Several polyamides contain the amino acid cysteine, which was prepared using different techniques and used in many applications. The use of water-soluble polyamides bearing primary amino side chains as a drug delivery system was one of the most significant applications. These polymers were manufactured by polymerization via N-protected L-cysteine I chloride and aliphatic diamines, supported by treatment with aqueous alkali solution. These polyamides include a two-side amino (NH_2) group for drug ligand binding [19]. These polymers can be rapidly biodegraded at the disulfide bonds by disulfide-thiol interactions.

Our study aims to load hypertension drug onto new polymers used in delivery systems. The nanocomposites were characterized in terms of %LE, zeta potential, and particle size. Furthermore, in vitro release studies were performed to study the nanocomposites' ability to deliver the amlodipine drug and form sustained release systems.

2. Materials and Methods

2.1. Materials. Amlodipine was purchased from Sigma-Aldrich. Buffer phosphate saline solution and sodium hydroxide were purchased from Chem Co. (England), and other chemicals, such as aluminum chloride and ferric chloride, were obtained from AZ chemicals (Karachi, Pakistan). Methanol was purchased from Sigma-Aldrich. The polymer used in this work was obtained from Dr. Dalia at Isra University.

2.2. Preparation of Polymer Nanoparticles. The solution of polymer was prepared by dissolving different amounts of the polymer (0.05, 0.125, and 0.2 g) in 30 mL of 0.1 M NaOH. The solution of FeCl_3 and AlCl_3 was prepared by dissolving different amounts of them (0.6, 1.5, 2.4 g) in 30 mL of distilled water. Finally, the solution of Amlop was prepared by dissolving 0.1 g in 20 mL of methanol.

Preparation of polymer nanoparticles was carried out by adding each selected amount of FeCl_3 and AlCl_3 to 30 mL of polymer solution. The pH of the polymer nanoparticles was adjusted to different levels (6, 8, and 10) by adding NaOH. The polymer nanoparticles were stirred for three hours and then centrifuged at 5000 rpm. The polymer nanoparticles were washed three times with distilled water and dried in an oven.

2.3. Preparation of Amlop-Polymer Nanocomposites. Amlop-polymer nanocomposites were prepared by the following method. The solution of amlodipine was mixed with the polymer solution. The two cross-linkers (FeCl_3 and AlCl_3) were added to the amlodipine-polymer mixture solution. The pH was adjusted at (6, 8, 10) by using 0.1 NaOH. Amlop-polymer nanocomposites were stirred for three hours and then centrifuged at a speed of 5000 rpm for 20 min. The Amlop-polymer nanocomposites were washed three times with distilled water and dried in an oven.

2.4. Determination of Loading Efficiency (%LE). The centrifugation technique was used to isolate the supernatant from the prepared nanocomposites. This process has several steps: the sample was centrifuged (Hettich Universal 30 RF, Germany) at 5000 rpm for 20 min. The free drug in the supernatant was calculated from the absorbance at a λ_{max} of 330 nm measured with an ultraviolet-visible spectrophotometer. The % LE of amlodipine was calculated with equation (1).

$$\% \text{Loading} = \frac{\text{Total mass of Amlop} - \text{Total mass of free Amlop}}{\text{Mass of nanocomposites}} \times 100. \quad (1)$$

2.5. In Vitro Release Study of Amlodipine from Nanocomposites. The in vitro rate of amlodipine release from nanocomposites was evaluated at pH 7.4 using phosphate-buffered saline solution (PBS) at a λ_{max} of 330 nm. A suitable amount of nanocomposite was inserted into the release media. The accumulated quantity of amlodipine released into solution was measured using an ultraviolet-visible spectrophotometer. The percentage rate of amlodipine release in PBS was determined with Equation (2):

$$\% \text{Release} = \frac{\text{Mass of Amlop at time } t}{\text{Mass of Amlop in nanocomposite}} \times 100. \quad (2)$$

2.6. Full Factorial Design (FFD) for Design of Experiments. In this work, we studied the effect of independent variables (polymer, Fe^{3+} , Al^{3+} , and pH) with three levels on the dependent variables (%LE, zeta potential, and particle size)

TABLE 1: Levels of polymer, FeCl₃, AlCl₃, and pH.

Parameter	Levels		
Polymer (g)	0.05	0.125	0.2
FeCl ₃ (g)	0.6	1.5	2.4
AlCl ₃ (g)	0.6	1.5	2.4
pH	6	8	10

(Table 1). The 52 nanocomposites parameters were designed by using FFD. The %LE, zeta potential, and particle size data are shown in Table S1.

2.7. Experimental Section. Ultraviolet–visible spectrophotometry is a common method used widely to qualitatively and quantitatively characterize samples. To quantitatively measure the drug release, a Shimadzu UV-1601 spectrophotometer at Isra University was used. In addition, Fourier transform infrared spectroscopy (FTIR) was applied to identify functional groups and chemical bonds existing in a molecule depicted from the infrared absorption spectrum obtained. The Fourier transform infrared spectra were obtained within 400 and 4000 cm⁻¹ on a Perkin Elmer with 4 cm⁻¹ resolution, with 0.01 g of sample. The particle size and zeta potential of the Amlop-polymer nanocomposites were evaluated. Dynamic light scattering was performed with a Zetasizer (Malvern, UK) at Hikma Pharmaceutical Manufacturing. The powder X-ray diffraction (PXRD) technique was used in the range 5–70° with an XRD D5005 diffractometer with CuK α radiation (Siemens, Munich, Germany). Scanning electron microscopy (FE-SEM) was used using a Zeiss LEO 1550 (Jena, Germany) instrument.

3. Results and Discussion

3.1. Response Surface Regression Analysis Using Full Quadratic. Table 2 shows all data collected from the lab work. The factors are statistically validated as models: first, a linear model including (Al³⁺, Fe³⁺, polymer, pH); second, a square model including (Al*Al); and third, a two-way interaction model including (Al*Fe, Al*polymer, Al*pH, Fe*polymer, Fe*pH, polymer*pH) were fitted using Minitab software for loading efficiency, zeta potential, and particle size.

Table 2 displays the ANOVA table for %LE, particle size, and zeta potential given in the proposed models. Therefore, a *P* value less than 0.05 indicates that the model is significant at the 95% confidence level. The lack-of-fit error values for the LE and zeta potential models are nonsignificant (0.336, 0.117, and 0.310), meaning that the suited model is accurate in determining the response. Mathematical models were created to select the proper values of the Amlop-polymer nanocomposites.

The coefficient of determination (R^2) is a statistical measure in a regression model used to determine the proportion of variance in the dependent variable (%LE, particle size, and zeta potential) that can be explained by the independent variable (Al, Fe, polymer, and pH). In this work, R^2 shows how

well the data fit the regression model (the goodness of fit) (Table S2 and Figure S1, SI).

3.2. Pareto Charts of the Effect for %LE, Particle Size, and Zeta Potential. Based on a graph and the ordering of the factors from the most impacting to the least impacting, when lines are viewed as columns that pass the point of reference, these lines (columns) are classified as statistically important impacts. Figure 1(a) shows the effect of several factors on % LE, including Fe, Al, Al*Fe, pH, Al*Al, Al*pH, polymer, and Fe*polymer. Specifically, two factors (Fe and Al) have the greatest effect on % LE. On the other hand, from Figure 1(c), there are six factors that are statistically significant for zeta potential (pH, Al*Al, polymer, Al, Fe, Fe*polymer). Specifically, the pH factor is considered to have the greatest statistically significant impact on the zeta potential. For the particle size aspect, based on Figure 1(b), all the factors was significant effect on the particle size, and there are two factors (Al*Fe, Al*polymer) that have the most statistically significant impact on particle size.

3.3. Residual versus Observation Order and Fitted Value. The residual versus observation order was used to verify the assumption that the residuals are independent from one another. Independent residuals show no trends or patterns when displayed in time order. Based on Figure S2, SI, the residual versus order of the three dependent variables demonstrates that there is no discernible trend in the plots. As a result, there was no chance of systemic errors in the model.

The residuals versus fits plot was used to verify the assumption that the residuals are randomly distributed. Ideally, the points should fall randomly on both sides. Figure S3, SI, residuals versus fits of three dependent variables, indicates that this model is ideal for the data because the points in a residual plot are randomly distributed on the horizontal axis.

3.4. Half-Normal Plots of the Standardized Effects. Consequently, according to the previously stated details and information, a half-normal plot is useful for determining the significance and nonsignificant of the results on the plot. Figure 2(a) indicates that the factor Fe has a highly significant impact on %LE, while the factor Al*Fe shows a greater effect on the particle size (Figure 2(b)), and the factor pH mainly affects zeta potential (Figure 2(c)). There are three factors (Al*polymer, Fe*pH, and polymer*pH) that do not have a statistically significant impact on the response, except on particle size.

3.5. Main Effect Plots for Loading Efficiency, Particle Size, and Zeta Potential. The influence of each variable at various levels of concentrations, which are linked to each other by a line on the result, can be explained using the main effects graph. In addition, this type of plot demonstrates the effects of increasing or decreasing the concentration of each factor on loading efficiency, particle size, and zeta potential.

Figure 3(a) shows the %LE by the main effects plot for the effect of Al. Initially, with increasing amounts of Al, the loading efficiency showed a moderate change even when the level of Al reached 1.6 g. After that, when the level of Al

TABLE 2: ANOVA table for % LE, particle size, and zeta potential.

LE model	DF	Adj SS	Adj MS	F-value	T-value	P-value	VIF
Model	11	3593.37	326.67	75.51		0.000	
Linear	4	3227.12	806.78	186.48		0.000	
Al	1	812.55	812.55	187.81	13.70	0.000	1.21
Fe	1	2634.97	2634.97	609.05	24.68	0.000	1.13
Polymer	1	32.09	32.09	7.42	2.72	0.011	1.15
pH	1	128.96	128.96	29.81	-5.46	0.000	1.18
Square	1	63.09	63.09	14.58		0.001	
Al*Al	1	63.09	63.09	14.58	3.82	0.001	1.01
2-way interaction	6	370.27	61.71	14.26		0.000	
Al*Fe	1	249.01	249.01	57.56	7.59	0.000	1.21
Al*polymer	1	0.80	0.80	0.18	-0.43	0.671	1.12
Al*pH	1	41.99	41.99	9.70	-3.12	0.004	1.11
Fe*polymer	1	21.92	21.92	5.07	2.25	0.032	1.15
Fe*pH	1	0.45	0.45	0.10	-0.32	0.748	1.18
Polymer*pH	1	8.68	8.68	2.01	-1.42	0.167	1.07
Error	31	134.12	4.33				
Lack-of-fit	4	20.16	5.04	1.19		0.336	
Pure error	27	113.96	4.22				
Total	42	3727.49					
Size model							
Model	11	268,342	24,395	60.00	15.30	0.000	
Linear	4	74,622	18,655	45.88		0.000	
Al	1	17,902	17,902	44.03	6.64	0.000	1.08
Fe	1	2033	2033	5.00	-2.24	0.033	1.12
Polymer	1	39,970	39,970	98.30	-9.91	0.000	1.13
pH	1	23,219	23,219	57.11	7.56	0.000	1.13
Square	1	10,611	10,611	26.10		0.000	
Al*Al	1	10,611	10,611	26.10	5.11	0.000	1.06
2-way interaction	6	159,695	26,616	65.46		0.000	
Al*Fe	1	105,767	105,767	260.13	-16.13	0.000	1.63
Al*polymer	1	59,821	59,821	147.13	12.13	0.000	1.83
Al*pH	1	9202	9202	22.63	-4.76	0.000	1.93
Fe*polymer	1	7306	7306	17.97	4.24	0.000	1.97
Fe*pH	1	13,036	13,036	32.06	-5.66	0.000	1.87
Polymer*pH	1	3396	3396	8.35	2.89	0.007	1.68
Error	30	12,198	407				
Lack-of-fit	3	2351	784	2.15		0.117	
Pure error	27	9847	365				
Total	41	280,540					
Potential model							
Model	11	22725.5	2066.0	492.87	-5.05	0.000	
Linear	4	19117.2	4779.3	1140.19		0.000	
Al	1	65.6	65.6	15.65	3.96	0.000	2.12
Fe	1	57.4	57.4	13.71	-3.70	0.001	1.81
Polymer	1	170.5	170.5	40.67	-6.38	0.000	1.20
pH	1	12388.1	12388.1	2955.42	-54.36	0.000	1.75
Square	1	283.5	283.5	67.63		0.000	
Al*Al	1	283.5	283.5	67.63	8.22	0.000	1.07

TABLE 2: Continued.

LE model	DF	Adj SS	Adj MS	F-value	T-value	P-value	VIF
2-way interaction	6	62.1	10.4	2.47		0.049	
Al*Fe	1	7.5	7.5	1.79	1.34	0.192	1.92
Al*polymer	1	0.5	0.5	0.11	-0.34	0.738	1.20
Al*pH	1	8.8	8.8	2.10	1.45	0.159	1.62
Fe*polymer	1	31.0	31.0	7.41	-2.72	0.011	1.19
Fe*pH	1	2.2	2.2	0.51	-0.72	0.480	1.77
Polymer*pH	1	0.2	0.2	0.05	-0.23	0.818	1.08
Error	27	113.2	4.2				
Lack-of-fit	3	15.4	5.1	1.26		0.310	
Pure error	24	97.8	4.1				
Total	38	22838.6					

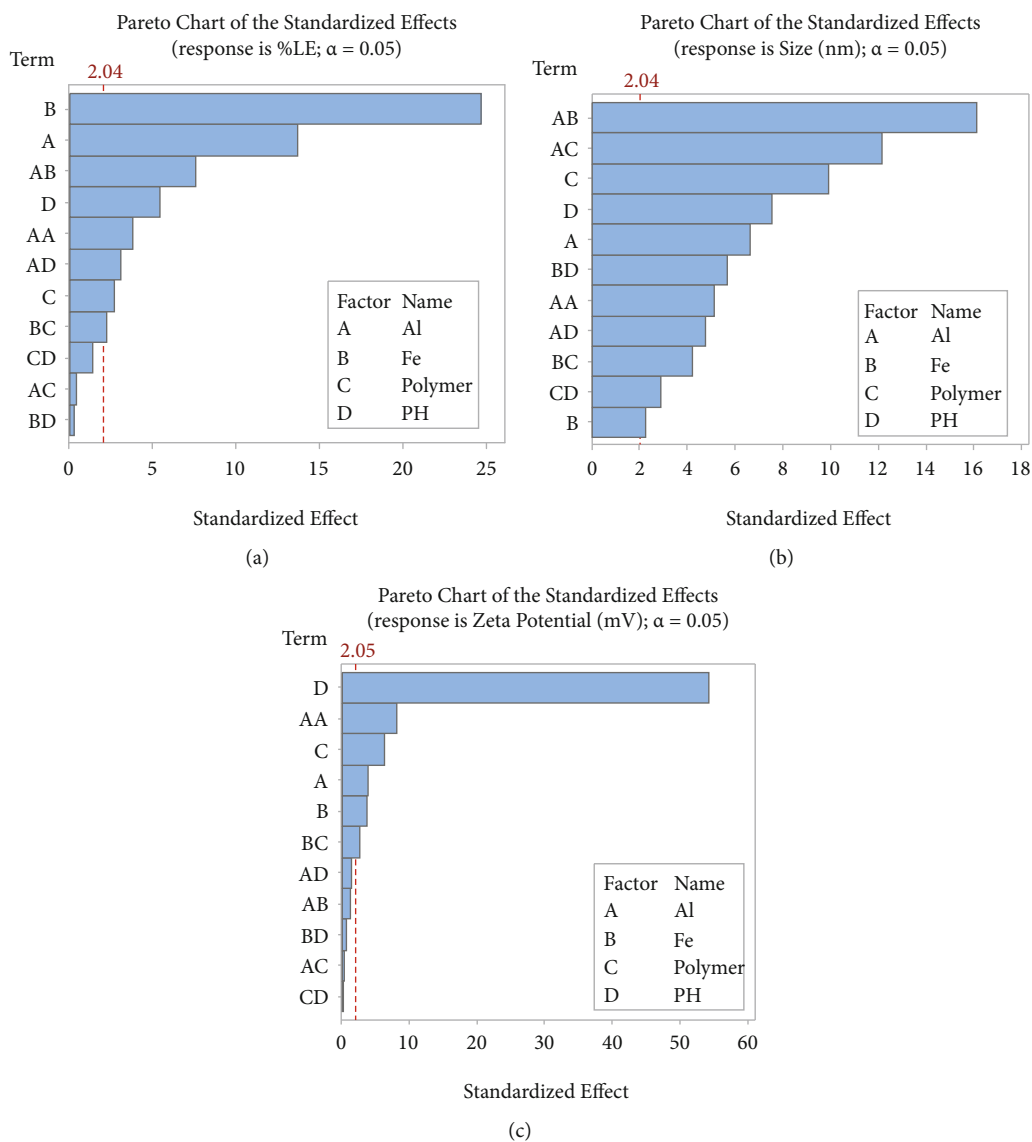


FIGURE 1: (a) Pareto charts showing the impact for %LE, (b) particle size, and (c) zeta potential.

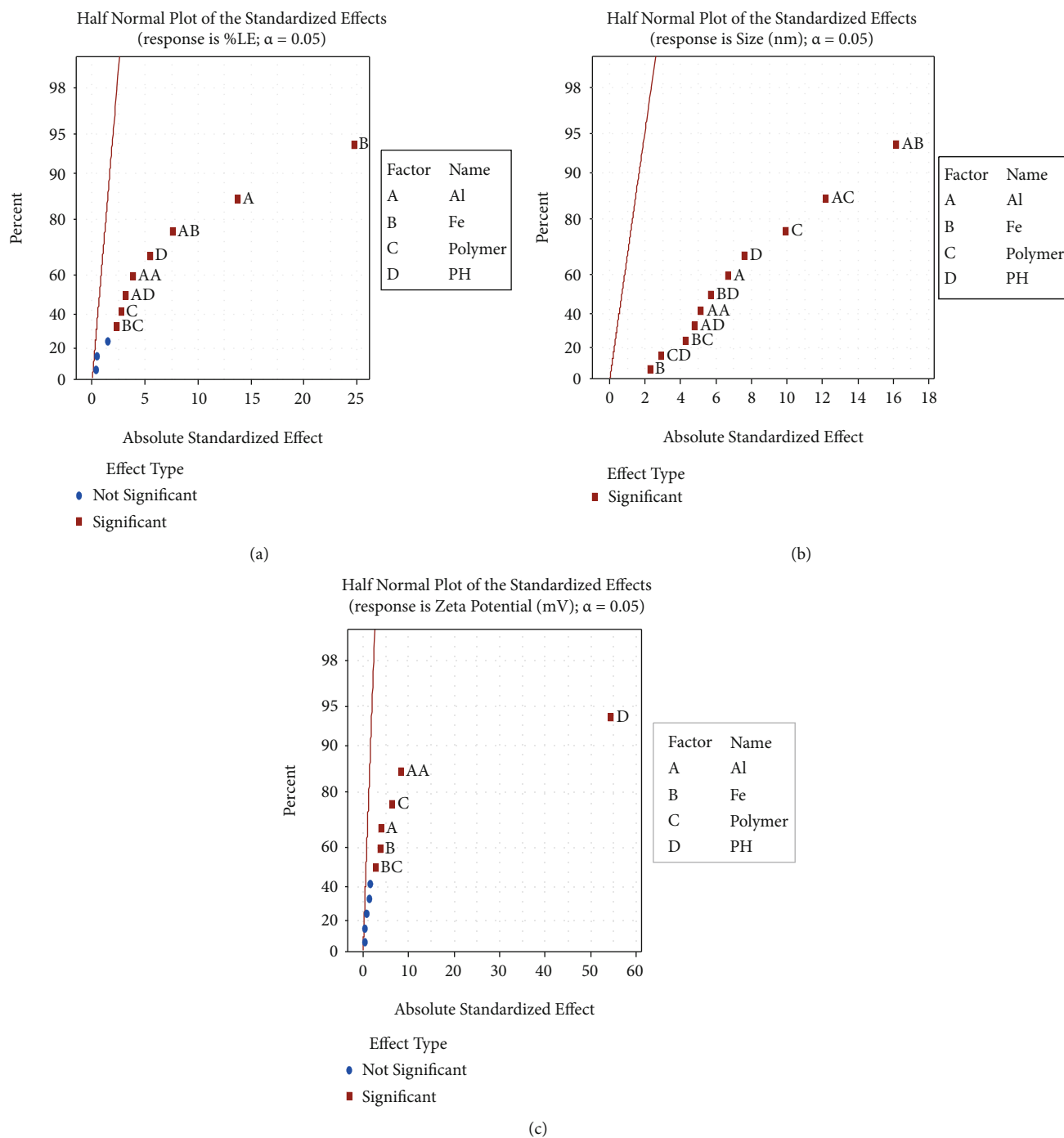


FIGURE 2: (a) Half normal plot of the standardized effects for %LE, (b) particle size, and (c) zeta potential.

increased more than 1.6 g, the loading efficiency began to rise. Figure 3(a) also shows the effect of Fe as a cross-linker on %LE. The loading efficiency rapidly increased with increasing levels of Fe, which indicates that both cross-linkers have a main effect on %LE. This is due to the polymer chains being linked to the drug by covalent or ionic bonds, resulting in highly complex expansion and a network structure [9].

In addition, Figure 3(a) shows that the polymer had a very weak effect on loading efficiency by increasing the %LE with increasing concentration of that drug as expected

due to the covalently bound and mechanically encapsulated forms of the polymer with the drug; this improves the stability and increases the loading of the drug [10]. Figure 3(a) also shows the relation between %LE and pH value. From the figure, it is clear that increasing the pH level will decrease %LE, which is likely due to the change in pH from 6 to 10 decreasing the negative charge of the polymer, which will negatively affect %LE.

Figure 3(b) shows the main effects plots for particle size. The figure shows that increasing the concentration of (Al)

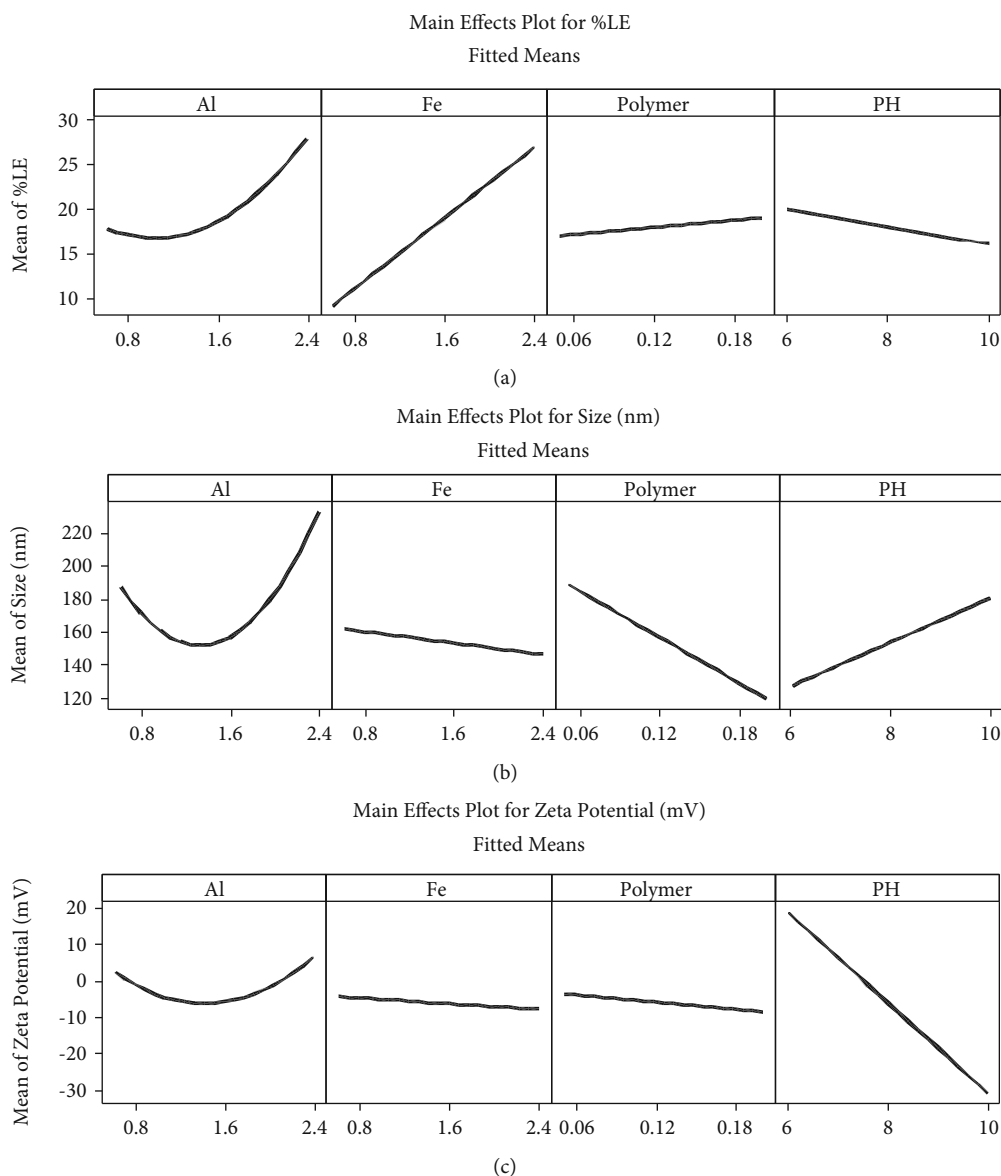


FIGURE 3: (a) Main effects plot for % LE, (b) particle size, and (c) zeta potential.

up to 1.6 g leads to a decrease in particle size. Then, when the level of Al is increased more than 1.6 g, the particle size grows. Figure 3(b) also shows the effect of Fe. According to the figure, using a concentration of Fe from 0.8 to 2.4 g, will decrease the particle size. Similar to Fe, the concentration of polymer indirectly affected particle size. Particle size decreased from 180 to 120 nm with an increase in the concentration of polymer from 0.06 up to 0.18 g. In addition, there is a direct relationship between pH and particle size; when increasing the pH from 6 to 9, the particle size began to increase from 130 to 180 nm.

In terms of zeta potential shown in the main effects plots, Figure 3(c) shows the zeta potential started to decrease marginally when the concentration of Al was increased up to 1.6 g. Then, after increasing the level of Al more than 1.6 g, the zeta potential started to rise gradually from 4 to 28 mV. Figure 3(c) shows that an increase in concentrations of Fe

and polymer does not have a significant impact on zeta potential. However, there is an inverse relationship between the pH and zeta potential; increasing the level of pH from 6 to 10 leads to a decrease in the zeta potential from 30 to 6 mV.

3.6. Interaction Plots for %LE, Zeta Potential, and Particle Size. Interaction plots are used to demonstrate how any factor influences the relation of the interaction with the next factor. This graph shows the various levels of one factor on the x-axis and an information line of the various levels of the second factor on the y-axis. When the curves or lines are parallel, that indicates there is no interference and interaction between factors. However, if the lines are not parallel, there is an interaction between factors. Figure 4(a) shows the interaction plot for %LE by showing the relation between Al with every variable (Fe, polymer, and pH) according to the various level of each.

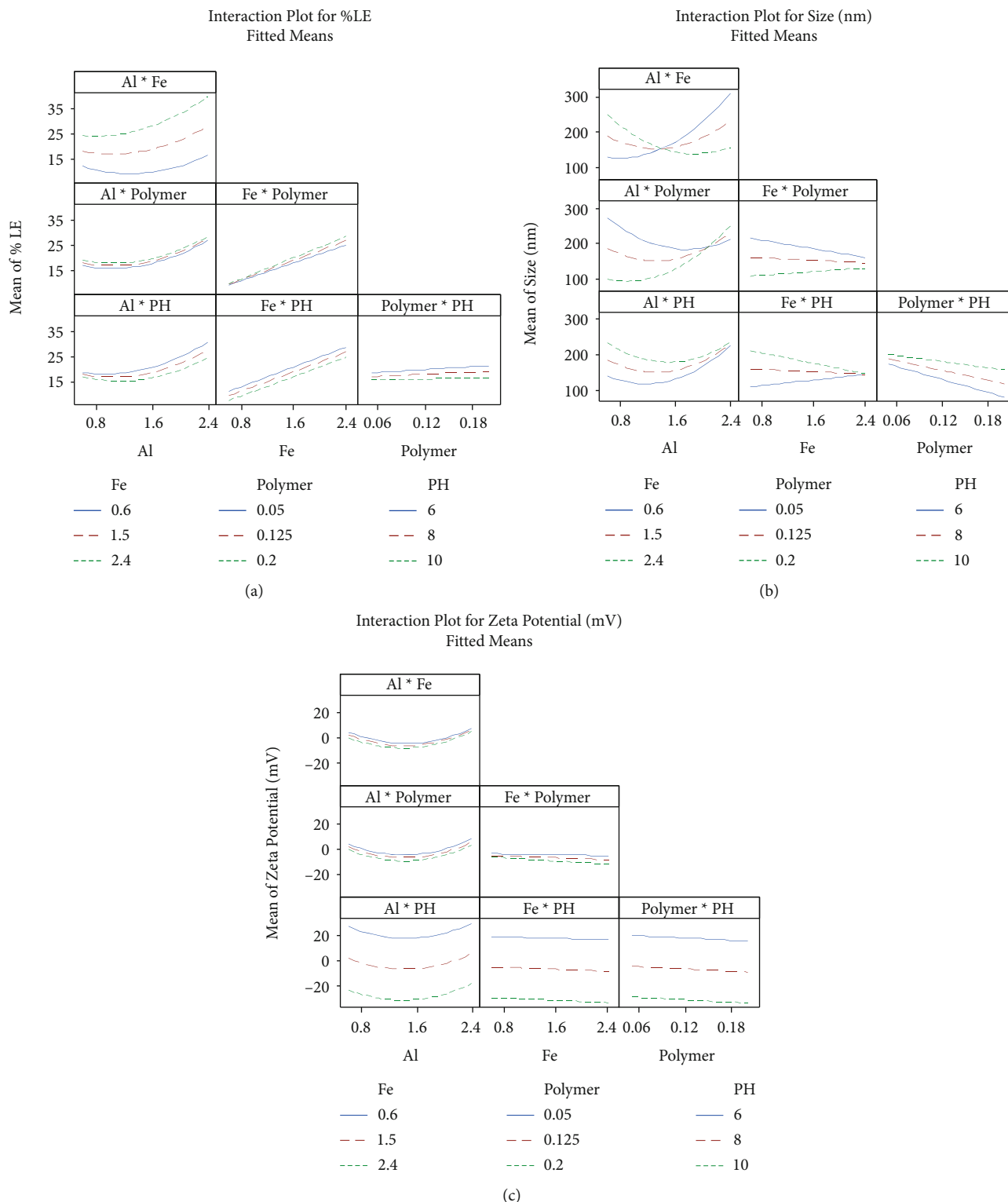


FIGURE 4: (a) Interaction plots for %LE, (b) particle size, and (c) zeta potential

The resulting lines or curves are not parallel, suggesting that there are significant interactions and contact between them. In addition, there is a significant interaction between Fe with polymer and Fe with pH. However, there is no interaction relationship between the polymer with pH because the lines are parallel and not in contact.

Figure 4(b) shows the interaction plot for particle size by showing the relation between Al with Fe, polymer, and pH. For all these factors, the lines or curves are not parallel, suggesting that there are significant interactions and contact between them.

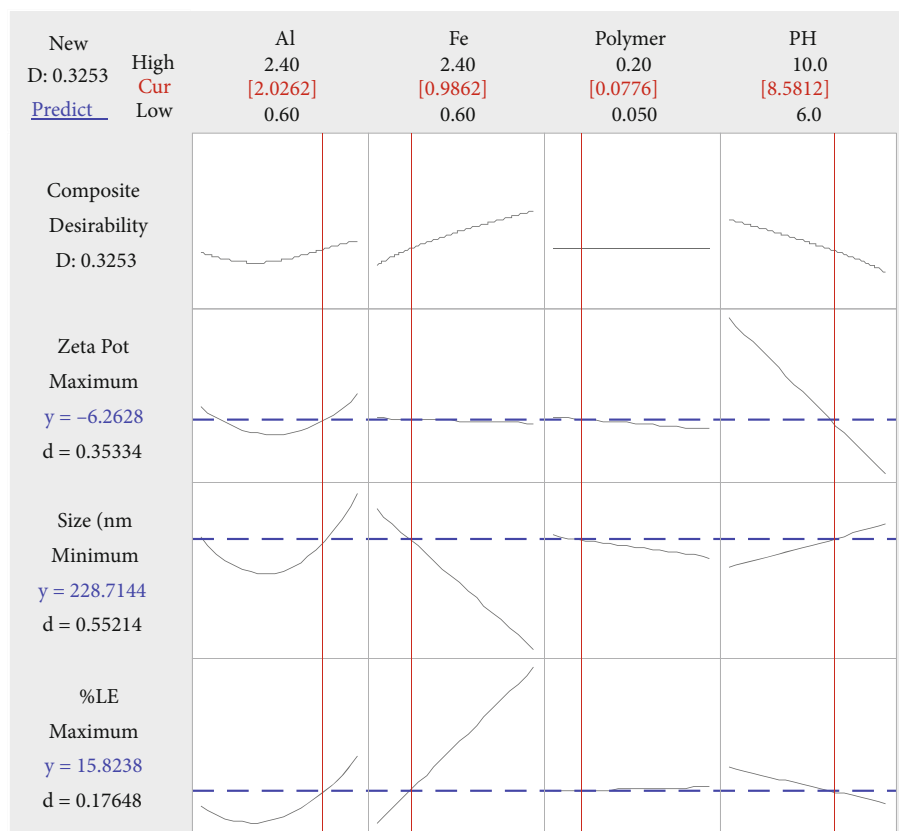


FIGURE 5: The optimized concentrations for response factors %LE, particle size, and zeta potential.

TABLE 3: Comparative results between observed and predicted response values of variables of optimized formulation.

Concentrations	Experimental response	Predicted values	Observed values	Bias (%)
Al (2.4 g)	LE (%)	40.5%	35.1%	-
Fe (2.4 g)				13.33%
Polymer (0.05 g)	Particle size (nm)	151 nm	170 nm	12.58%
pH = 6	Zeta potential (mV)	33.92 mV	35.1 mV	3.47%
Al (1.58 g)	LE (%)	19.7%	22.1%	12.18%
Fe (1.60 g)	Particle size (nm)	156 nm	168 nm	7.69%
Polymer (0.12 g)	Zeta potential (mV)	3.33 mV	3.29 mV	-1.20%
pH = 7.8				
Al (2.02 g)	LE (%)	15.8%	20.2%	27.84%
Fe (0.99 g)	Particle size (nm)	229 nm	238 nm	3.93%
Polymer (0.08 g)	Zeta potential (mV)	6.26 mV	5.97 mV	-4.63%
pH = 8.6				

%Bias was calculated as ((observed value - predicted value)/predicted value) × 100.

Figure 4(c) shows the interaction plot for zeta potential, showing the relation between Al with Fe and polymer and between Fe with polymer. The lines or curves are not parallel, suggesting that there are significant interactions and contact between them. However, there was no evidence of a significant interaction between Al with pH, Fe with pH, and polymer with pH because the lines are parallel.

3.7. Optimization of the Three Models. Figure 5 was taken from the software. These new values for each variable (polymer, FeCl₃, AlCl₃, and pH) were obtained by moving the red

line. Changing the values of the previous four factors would provide new data predicted for loading efficiency, particle size, and zeta potential. After preparing the samples in the laboratory, experimental results were obtained for loading efficiency, particle size, and zeta potential. After that, we calculated and analyzed the differences between the predicted and experimental results using the bias equation.

3.8. Validation of the Three Models. Table 3 represent the relation between the expected (predicted) values and experimental values according to the questions in Table

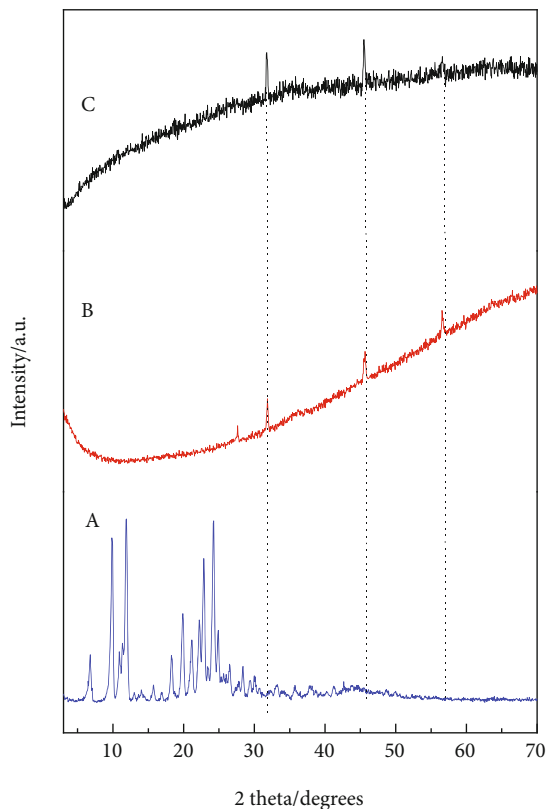


FIGURE 6: Powder X-ray diffraction patterns of the (a) Amlodipine, (b) polymer nanoparticles and (c) Amlop-polymer nanocomposite.

S3. The values of bias were -13.33% , 12.58% , and 3.47% for the first sample (Al = 2.4 g, Fe = 2.4 g, polymer = 0.05 g, and pH = 6). Additionally, the values of bias were 12.18% , 7.69% , and -1.20% for the second sample (Al = 1.58 g, Fe = 1.60 g, polymer = 0.12 g, and pH = 7.8). For the third sample (Al = 2.02 g, Fe = 0.99 g, polymer = 0.08 g, and pH = 8.6), the values of bias were 27.84% , 3.93% , and -4.63% . These conclusions prove the accuracy and validity of the models used in this study, as there is no statistically significant difference between expected (predicted) and experimental values.

3.9. Characterization of Amlop-Polymer Nanocomposites

3.9.1. X-Ray Diffraction (XRD). The XRD patterns of the pure amlodipine, polymer nanoparticles and Amlop-polymer-nanocomposite are presented in Figure 6. Amlodipine showed the characteristic sharp peaks at 2θ values of 9.85 , 11.85 , 22.85 , and 24.25° , which indicated the crystalline property of the amlodipine drug [20, 21]. The polymer nanoparticles exhibited one wide broad peak with three prominent small sharp peaks at 31.85 , 45.65 , and 56.55° . The nature of the peak indicates the semicrystallinity of the polymer [22]. Interpretation of the XRD patterns of the amlopolymer nanocomposite indicated that there was a tiny shift in the peak heights without a change in the d -spacing of the peaks. The disappearance of drug peaks in the nanocomposites indicates that the drug was

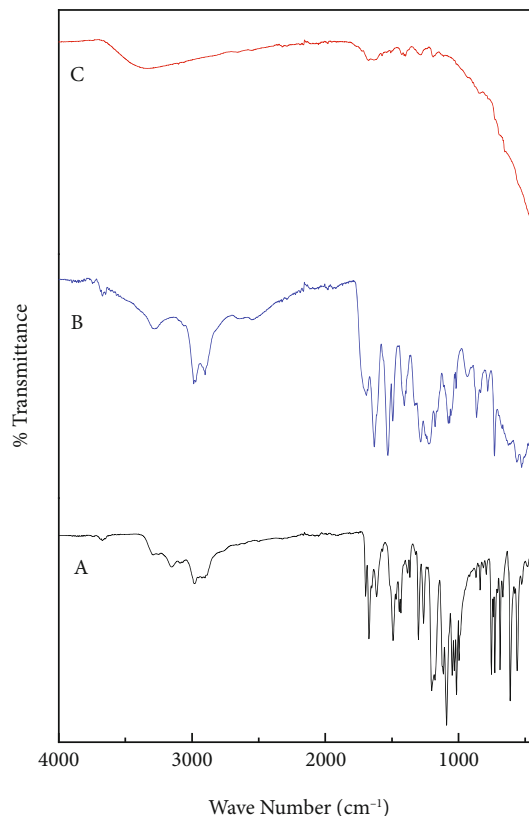


FIGURE 7: FTIR spectrum of (a) amlodipine, (b) polymer, and (c) Amlop-polymer nanocomposite.

incorporated between the polymer molecules and amorphous [23, 24].

3.9.2. Fourier Transform Infrared (FT-IR). The FTIR spectrum of amlodipine is shown in Figure 7(a). As shown in the figure, the band at 3000 cm^{-1} is due to hydroxide OH groups, while the band at 3310 cm^{-1} can be attributed to N-H groups [25]. The band recorded at 1670 cm^{-1} is related to the stretching of the C=O group. The band at 1613 cm^{-1} is due to C=C in the aromatic region [26]. The C-O group shows peaks at 1017 cm^{-1} that are related to $\nu(\text{C=O})$ stretching [27, 28].

As can be observed in the FTIR spectrum of the polymer (Figure 7(b)), a broad band at 3300 cm^{-1} could be attributed to the N-H stretching vibration. The band at 2991 cm^{-1} is due to the vibration of the O-H group. The peak at 1715 cm^{-1} is due to the vibration of C=O of the amide group [29]. A band at 1626 cm^{-1} is due to the asymmetric vibration mode of COO^- , and another band at 1406 cm^{-1} is due to the symmetric vibration of COO^- [30]. The band at 565 cm^{-1} is due to the vibration of the S-S group [31]. In addition, the methyl group (alkanes) has a C-H stretching peak at 2988 cm^{-1} [32].

The FTIR spectrum of the Amlop-polymer nanocomposite is shown in Figure 7(c) and shows the characteristic bands of amlodipine. This indicates that amlodipine has been incorporated into the polymer nanoparticles. The two peaks of Fe^{+3} and Al^{+3} appear at wavenumbers 510 and 1082 cm^{-1} , respectively [33].

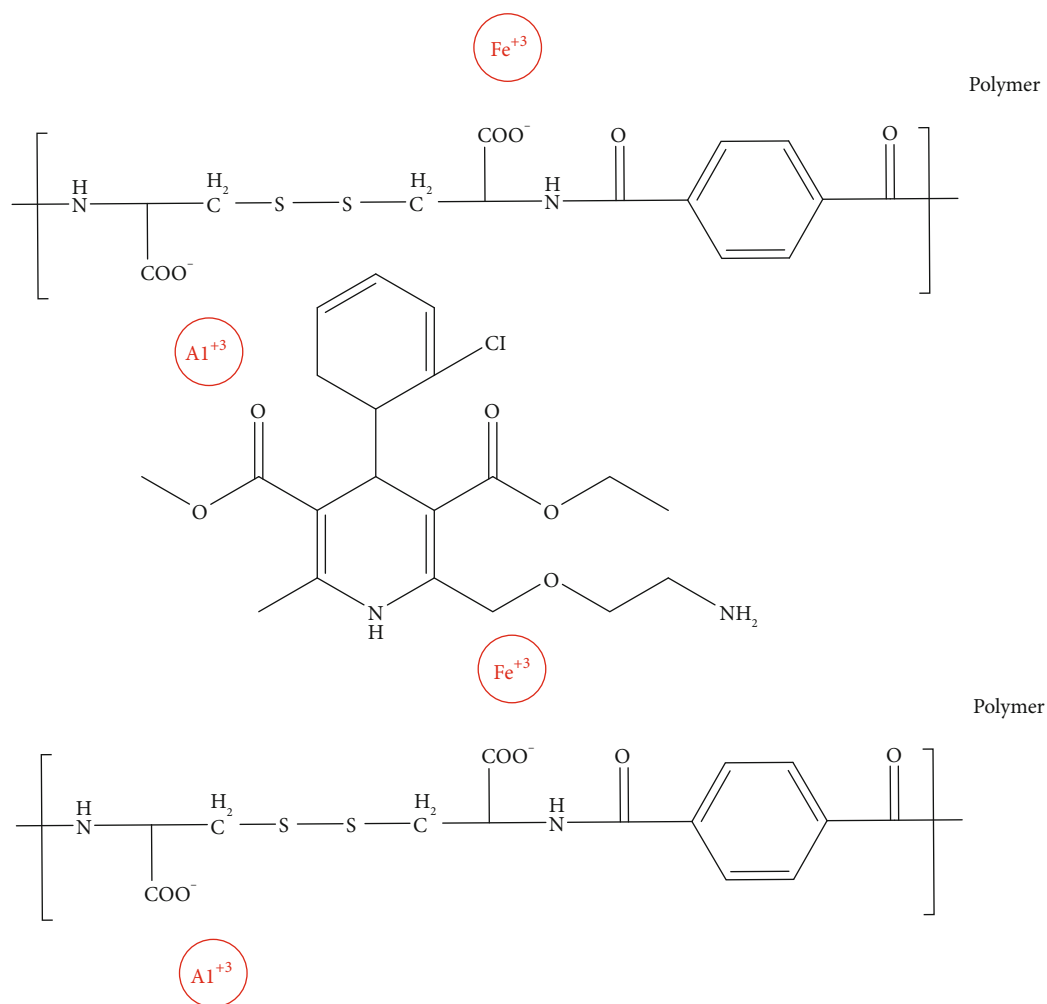


FIGURE 8: The interaction in Amlopolymer nanocomposites.

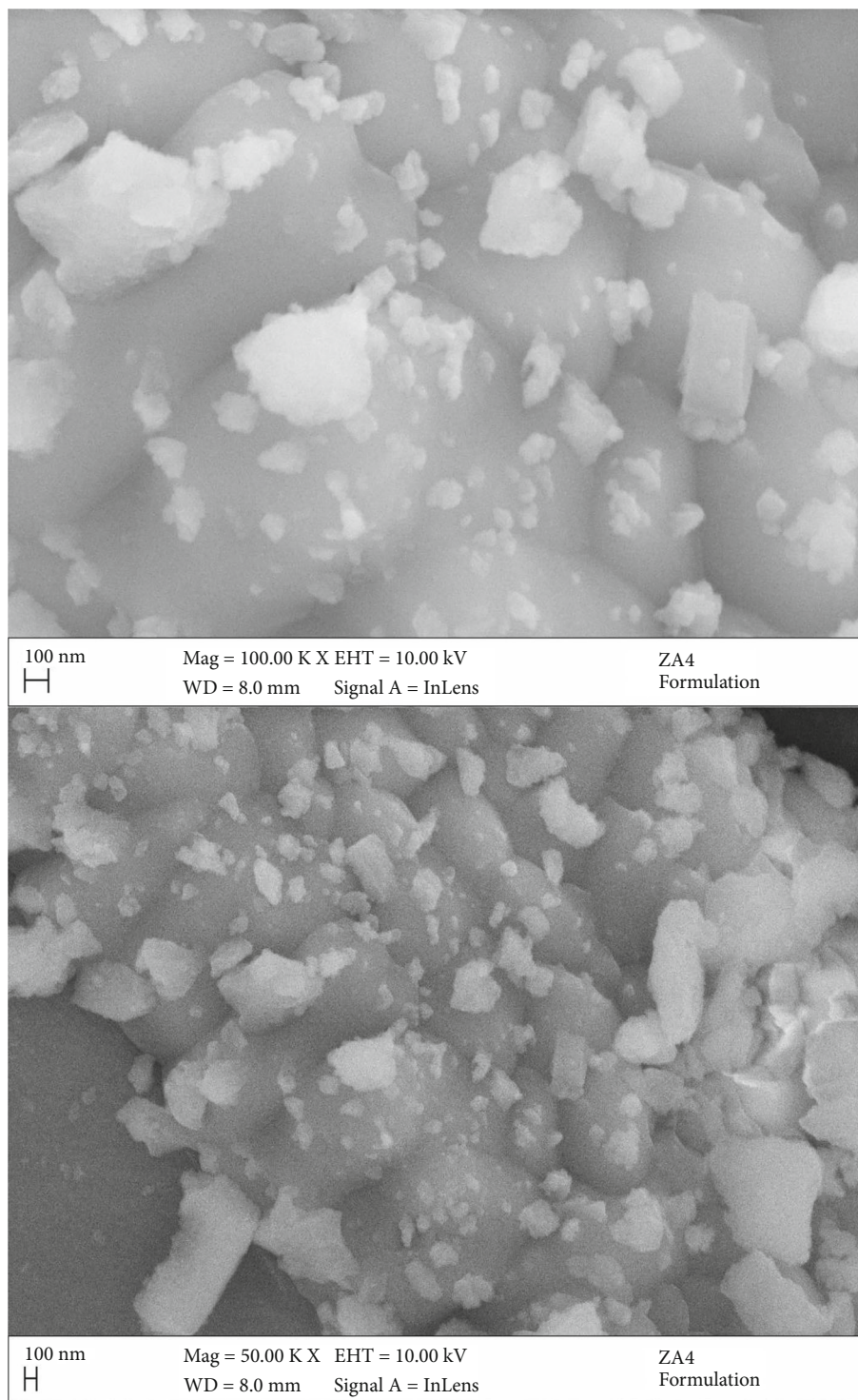
3.9.3. The Interaction between Amlopolymer and Polymer in Nanocomposites. Since the polymer used in this work contains carboxylic acid and amine groups, it will take on three different charges: positive when using a pH less than the $pK_a = 4.1$ of the polymer, neutral when using a pH equivalent to the pK_a of the polymer, and negative when using a pH higher than the pK_a of the polymer [32]. In addition, the amlodipine drug has a pK_a value of 9.3 [34]. Therefore, when using a pH between 9.3 and 11, the drug will have a neutral charge (NH_2). When using a pH between 3 and 9.3, the drug will take on a positive charge (NH_3^+). During the preparation of the 52 samples in this work, we used three different pH levels: 6, 8, and 10. This result indicates that the drug in the nanocomposite prepared at pH = 10 has NH_2 groups, while the nanocomposites prepared at pH = 6 and 8 have positive charges. According to that, the drug was encapsulated inside the polymer and attached by hydrogen bonds (Figure 8).

3.9.4. Field Emission Scanning Electron Microscopy (FE-SEM). As shown in Figure 9, FE-SEM was used to identify

the particle size and morphology of the prepared nanocomposites. The results showed that our nanocomposites have an average particle size of approximately 130 nm.

3.9.5. In Vitro Release Study of Amlopolymer from Nanocomposites. The release profiles of amlodipine from the Amlopolymer nanocomposites are shown in Figure 10. Amlodipine release from the nanocomposite started at 12% and reached 85% over 24 hours.

The release of drugs from nanoparticles is regulated by many mechanisms. Swelling of hydrogel beads is one of the key processes that leads to the release of a drug by enabling water to flow inside the polymer and then starting the release of the drug during polymer breakdown [35]. The diffusion-controlled release systems were a possible mechanism of amlodipine release from polyamides and disulfide polymers. The drug is held in a core that is covered by a polymer. Therefore, the drug diffuses from the core to the outside polymer [36]. As a result, the bonds between the medication and the polymer start breaking [37].



(a)

FIGURE 9: Continued.

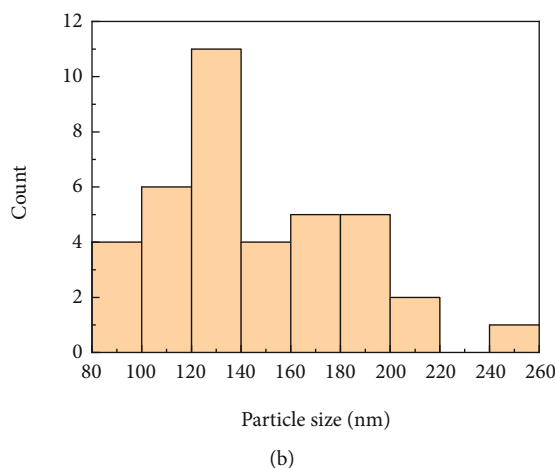


FIGURE 9: Scanning electron microscope images of (a) Amlop-polymer nanocomposite and (b) the histogram data for Amlop-polymer nanocomposite.

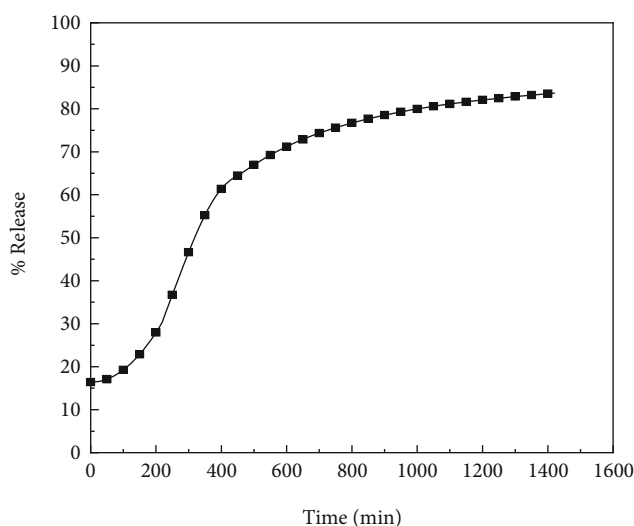


FIGURE 10: *In vitro* release of Amlodipine from Amlop-polymer nanocomposites in PBS at pH 7.4.

4. Conclusion

This research aims to use polyamide-polysulfide nanoparticles as drug delivery systems. Amlodipine (Amlop) was used as a model to form Amlop-polymer nanocomposites. In this work, we investigated the effect of independent variables (polymer, Fe^{3+} , Al^{3+} , and pH) on the dependent variables (%LE, zeta potential, and particle size). This nanocomposite was evaluated in the current study by using Minitab 18 software. The amlodipine in this study was used as a model of the drug loaded on the novel polymer with polyamides and disulfide linkages. The study obtained a particle size between 88 and 380 nm, a zeta potential between -25.4 and 34.8 mV and a loading efficiency of approximately 35%. The formulations prepared are a better therapeutic delivery system for amlodipine to improve its bioavailability, absorption, stability, and drug release profile, exhibiting extended release over more than 24 hours and better therapeutic effect by reducing

side effects. Therefore, the study indicates that the polymer with amlodipine has the most significant impact on loading efficacy, particle size, and zeta potential.

Data Availability

Data are available on request from corresponding author Dr. Samer Hasan Hussein-Al-Ali.

Conflicts of Interest

The authors declare that they have no conflicts of interest.

Acknowledgment

The author would like to thank the Faculty of Pharmacy at Isra University for provided funding for this research under grand number 6-23-2020/2021. This study was also supported by Hikma pharmaceuticals Research and development Department. Furthermore, the authors would like to acknowledge the institute of functional nanosystems for the permission to use their advanced facilities in UIM university (Germany).

Supplementary Materials

Table S1: the raw data which collected from lab work; Table S2 the R^2 values for the three models; Table S3 regression equations for the LE, particle size and zeta potential models; Figure S1 normal probability plots for %LE (A), particle size (B), and zeta potential (C). Figure S2 residual versus order of model for %LE (A), particle size (B), and zeta potential (C). Figure S3 residuals versus fits of model for %LE (A), particle size (B), and zeta potential (C). Figure S4 contour and surface plots for % LE against Fe^{3+} , Al^{3+} , pH and polymer variables; Figure S5 contour plots and surface plots for particle size against Fe^{3+} , Al^{3+} , pH and polymer variables; Figure S6 contour plots and surface plots for zeta potential against Fe^{3+} , Al^{3+} , pH and polymer variables. (*Supplementary Materials*)

References

- [1] M. Anwar, F. Muhammad, and B. Akhtar, "Biodegradable nanoparticles as drug delivery devices," *Journal of Drug Delivery Science and Technology*, vol. 64, article 102638, 2021.
- [2] J. Smith, "Conducting polymers as drug release systems," in *Nano-and Microfabrication Techniques in Drug Delivery: Recent Developments and Future Prospects*, Springer Nature, 2022.
- [3] P. Bhatt, S. Trehan, N. Inamdar, V. K. Mourya, and A. Misra, "Polymers in drug delivery: an update," in *Applications of Polymers in Drug Delivery*, pp. 1–42, Elsevier, 2021.
- [4] J. V. Suman, K. K. Cheepurupalli, and H. L. Allasi, "Design of polymer-based trigate nanoscale FinFET for the implementation of two-stage operational amplifier," *International Journal of Polymer Science*, vol. 2022, 2022.
- [5] K. J. Gandhi, S. V. Deshmane, and K. R. Biyani, "Polymers in pharmaceutical drug delivery system: a review," *International Journal of Pharmaceutical Sciences Review and Research*, vol. 14, no. 2, pp. 57–66, 2012.
- [6] H. A. K. Sabbagh, Z. Abudayah, S. M. Abudoleh, J. A. Alkrad, M. Z. Hussein, and S. H. Hussein-al-Ali, "Application of multiple regression analysis in optimization of metronidazole-chitosan nanoparticles," *Journal of Polymer Research*, vol. 26, no. 8, pp. 1–14, 2019.
- [7] A. Hu, A. A. Alarfaj, A. H. Hiram et al., "Chitosan-sodium alginate-polyethylene glycol-crocin nanocomposite treatment inhibits esophageal cancer KYSE-150 cell growth via inducing apoptotic cell death," *Arabian Journal of Chemistry*, vol. 15, no. 6, article 103844, 2022.
- [8] M. S. Al-Qubaisi, A. Rasedee, M. H. Flaifel et al., "Characterization of thymoquinone/hydroxypropyl- β -cyclodextrin inclusion complex: application to anti-allergy properties," *European Journal of Pharmaceutical Sciences*, vol. 133, pp. 167–182, 2019.
- [9] H. A. K. Sabbagh, S. H. Hussein-al-Ali, M. Z. Hussein, Z. Abudayah, R. Ayoub, and S. M. Abudoleh, "A statistical study on the development of metronidazole-chitosan-alginate nanocomposite formulation using the full factorial design," *Polymers*, vol. 12, no. 4, p. 772, 2020.
- [10] N. M. Alkurdi, S. H. Hussein-al-Ali, A. Albalwi, M. K. Haddad, Y. Aldalahmed, and D. K. Ali, "Development and evaluation of a novel polymer drug delivery system using cromolyn-polyamides-disulfide using response surface design," *Journal of Chemistry*, vol. 2022, p. 19, 2022.
- [11] N. Strambeanu, L. Demetrovici, D. Dragos, and M. Lungu, "Nanoparticles: definition, classification and general physical properties," in *Nanoparticles' Promises and Risks*, pp. 3–8, Springer, 2015.
- [12] J. H. Sakamoto, A. L. van de Ven, B. Godin et al., "Enabling individualized therapy through nanotechnology," *Pharmacological Research*, vol. 62, no. 2, pp. 57–89, 2010.
- [13] H. Fares, J. J. DiNicolantonio, J. H. O'Keefe, and C. J. Lavie, "Amlodipine in hypertension: a first-line agent with efficacy for improving blood pressure and patient outcomes," *Open Heart*, vol. 3, no. 2, article e000473, 2016.
- [14] K. G. Bulsara and M. Cassagnol, "Amlodipine," in *StatPearls [Internet]*, StatPearls Publishing, 2021.
- [15] S. H. Alawdi, H. Eidi, M. M. Safar, and M. A. Abdel-Wahhab, "Loading amlodipine on diamond nanoparticles: a novel drug delivery system," *Nanotechnology, Science and Applications*, vol. 12, p. 47, 2019.
- [16] V. Chourasiya, S. Bohrey, and A. Pandey, "Formulation, optimization, and characterization of amlodipine besylate loaded polymeric nanoparticles," *Polymers and Polymer Composites*, vol. 29, 9 suppl, pp. S1555–S1568, 2021.
- [17] M. Uthaman and M. Koland, "Investigation of polymeric micellar nanoparticles of amlodipine besylate for transdermal delivery," *Journal of Young Pharmacists*, vol. 12, no. 4, pp. 314–320, 2020.
- [18] J. Abolhasani, A. Samadi, and M. H. Vahabzadeh, "Amlodipine-gold nanoparticles as a new "Turn off-on" sensor for the sensitive determination of methimazole," *Journal of Analytical Chemistry*, vol. 75, no. 3, pp. 402–408, 2020.
- [19] M. G. Meirim, E. W. Neuse, and F. Parisi, "Water-soluble polyamides as potential drug carriers. I. Poly(α,β -D,L-asparthrazide-co-D,L-ornithine)," *Macromolecular Chemistry and Physics*, vol. 175, no. 1, pp. 141–156, 1990.
- [20] G. Ananchenko, J. Novakovic, and J. Lewis, "Amlodipine Besylate," in *Profiles of Drug Substances, Excipients and Related Methodology*, H. G. Brittain, Ed., pp. 31–77, Academic Press, 2012.
- [21] M. Novac, A. M. Musuc, E. A. Ozon et al., "Design and evaluation of orally dispersible tablets containing amlodipine inclusion complexes in hydroxypropyl- β -cyclodextrin and methyl- β -cyclodextrin," *Materials*, vol. 15, no. 15, p. 5217, 2022.
- [22] S. K. Nagaraj, S. Shivanna, N. K. Subramani, and H. Siddaramaiah, "Revisiting powder X-ray diffraction technique: a powerful tool to characterize polymers and their composite films," *Journal of Materials Science*, vol. 4, pp. 1–5, 2016.
- [23] W. Qian, D. G. Yu, Y. Li, X. Y. Li, Y. Z. Liao, and X. Wang, "Triple-component drug-loaded nanocomposites prepared using a modified coaxial electrospinning," *Journal of Nanomaterials*, vol. 2013, p. 7, 2013.
- [24] H. Hosseinzadeh, S. Hosseinzadeh, S. Pashaei, N. Ghorbani, and R. Mazaherpour, "Synthesis of multiresponsive β -cyclodextrin nanocomposite through surface RAFT polymerization for controlled drug delivery," *Polymers for Advanced Technologies*, vol. 30, no. 11, pp. 2860–2871, 2019.
- [25] A. Rai and S. Sharma, "Preparation and evaluation of oral dispersible formulations of amlodipine besylate," *Asian Journal of Pharmaceutical Research and Development*, vol. 7, no. 5, pp. 43–56, 2019.
- [26] B. Gidwani, L. Patel, A. Gupta, and C. D. Kaur, "Ultra-violet spectrophotometric method for estimation and validation of amlodipine in bulk and tablet formulation," *Journal of Analytical & Pharmaceutical Research*, vol. 4, no. 00125, p. 10.15406, 2017.
- [27] P. Ramasubramaniyan, S. Palanichamy, V. M. Deepu, and M. Rajesh, "Formulation and evaluation of amlodipine besylate floating tablets," *Research Journal of Pharmaceutical, Biological and Chemical Sciences*, vol. 4, no. 4, pp. 15–33, 2013.
- [28] L. Szabo, V. Chiş, A. Pîrnău, N. Leopold, O. Cozar, and S. Orosz, "Spectroscopic and theoretical study of amlodipine besylate," *Journal of Molecular Structure*, vol. 924–926, pp. 385–392, 2009.
- [29] Y. Xue, A. Patel, V. Sant, and S. Sant, "Semi-quantitative FTIR analysis of the crosslinking density of poly(ester amide)-based thermoset elastomers," *Macromolecular Materials and Engineering*, vol. 301, no. 3, pp. 296–305, 2016.
- [30] S. H. H. Al Ali, M. Al-Qubaisi, M. Z. Hussein, M. Ismail, Z. Zainal, and M. N. Hakim, "Comparative study of Mg/Al and Zn/Al-layered double hydroxide-perindopril erbumine

- nanocomposites for inhibition of angiotensin-converting enzyme,” *International Journal of Nanomedicine*, vol. 7, p. 4251, 2012.
- [31] P. Sihota, R. N. Yadav, V. Dhiman, S. K. Bhadada, V. Mehandia, and N. Kumar, “Investigation of diabetic patient's fingernail quality to monitor type 2 diabetes induced tissue damage,” *Scientific Reports*, vol. 9, no. 1, pp. 1–11, 2019.
- [32] D. K. Ali, A. M. Al-Zuheiri, and B. A. Sweileh, “pH and reduction sensitive bio-based polyamides derived from renewable dicarboxylic acid monomers and cystine amino acid,” *International Journal of Polymer Analysis and Characterization*, vol. 22, no. 4, pp. 361–373, 2017.
- [33] M. A. González-Gómez, S. Belderbos, S. Yañez-Vilar et al., “Development of superparamagnetic nanoparticles coated with polyacrylic acid and aluminum hydroxide as an efficient contrast agent for multimodal imaging,” *Nanomaterials*, vol. 9, no. 11, p. 1626, 2019.
- [34] L. Settimo, K. Bellman, and R. Knegt, “Comparison of the accuracy of experimental and predicted pK_a values of basic and acidic compounds,” *Pharmaceutical Research*, vol. 31, no. 4, pp. 1082–1095, 2014.
- [35] B. Fonseca-Santos and M. Chorilli, “An overview of carboxymethyl derivatives of chitosan: their use as biomaterials and drug delivery systems,” *Materials Science and Engineering: C*, vol. 77, pp. 1349–1362, 2017.
- [36] A. Pramanik and S. Garg, “Design of diffusion-controlled drug delivery devices for controlled release of paclitaxel,” *Chemical Biology & Drug Design*, vol. 94, no. 2, pp. 1478–1487, 2019.
- [37] L. Serra, J. Doménech, and N. A. Peppas, “Engineering design and molecular dynamics of mucoadhesive drug delivery systems as targeting agents,” *European Journal of Pharmaceutics and Biopharmaceutics*, vol. 71, no. 3, pp. 519–528, 2009.